

Radiation and Roughness Effects on Nozzle Thermochemical Erosion in Solid Rocket Motors

Alessandro Turchi* and Daniele Bianchi†

University of Rome “La Sapienza,” 00184 Rome, Italy

Piyush Thakre‡

CD-adapco, Ltd., Melville, New York 11747

Francesco Nasuti§

University of Rome “La Sapienza,” 00184 Rome, Italy

and

Vigor Yang¶

Georgia Institute of Technology, Atlanta, Georgia 30332-0150

DOI: 10.2514/1.B34997

Surface roughness and radiation effects on the erosion behavior of a graphite nozzle are studied for both metallized and nonmetallized propellants. A validated numerical approach that relies on a full Navier–Stokes flow solver coupled with a thermochemical ablation model is used for the analysis. A modification of the Spalart–Allmaras turbulence model is implemented to account for surface roughness. Net radiative heat flux is considered in the surface energy balance at the nozzle interface. Two different simplified models are used to evaluate the integral emissivity of dispersed alumina particles. Individual and combined effects of roughness and radiation are analyzed. Surface roughness enhances the erosion rate for both metallized and nonmetallized propellants noticeably. The radiation influences the erosion rate of nonmetallized propellant more than the metallized one, mainly due to the different erosion regimes, kinetically controlled for the former and diffusion controlled for the latter.

Nomenclature

\mathcal{D}_{ij}	=	binary diffusion coefficient, m^2/s
D_{im}	=	effective diffusion coefficient, m^2/s
e_0	=	total specific energy, J/kg
h	=	enthalpy, J/kg
h_{eq}	=	equivalent sand grain roughness, m
\mathbf{j}	=	diffusional mass flux, $\text{kg}/\text{m}^2 \cdot \text{s}$
k	=	thermal conductivity, $\text{W}/\text{m} \cdot \text{K}$
\dot{m}	=	mass blowing rate per unit area, $\text{kg}/\text{m}^2 \cdot \text{s}$
N_s	=	number of species
p	=	pressure, N/m^2
$\dot{\mathbf{q}}$	=	heat flux, W/m^2
\dot{s}	=	erosion rate, m/s
T	=	temperature, K
t	=	time, s
u_τ	=	friction velocity
v	=	velocity component normal to surface, m/s
\mathbf{v}	=	flow velocity vector, m/s
\dot{w}	=	species source term, $\text{kg}/\text{m}^3 \cdot \text{s}$
x	=	mole fraction

y	=	mass fraction
α	=	absorptivity
ϵ	=	integral emissivity
η	=	inward (from solid to gas) coordinate normal to surface
μ	=	dynamic viscosity, $\text{kg}/\text{m} \cdot \text{s}$
ν	=	kinematic viscosity, m^2/s
ρ	=	density, kg/m^3
σ	=	Stefan–Boltzmann constant
$\dot{\omega}$	=	species source term in control surface, $\text{kg}/\text{m}^2 \cdot \text{s}$

Subscripts

b	=	bulk value
c	=	combustion chamber conditions
g	=	gas phase
i	=	species
s	=	solid state
w	=	gas properties at gas–solid interface
0	=	initial condition

Superscript

+	=	wall units
---	---	------------

I. Introduction

Ablative materials provide a reliable and relatively low-cost way to manage the extremely high heat fluxes that are normally encountered in a wide variety of aerospace applications. Reentry [1] and launch vehicles [2] provide some examples of the thermal protection system (TPS) application, in which ablation is used to mitigate harsh thermal and chemical conditions. The material response represents one of the key issues when working with ablative TPS.

One of the applications of TPS in launch vehicles is in solid rocket motor nozzles. In the nozzles, ablative material consumption depends on numerous factors including propellant composition, engine operating conditions, duration of firing, nozzle geometry and material properties, transport of reacting species, homogeneous reactions in the gas phase, and heterogeneous reactions at the nozzle surface. Specification of ablative material characteristics and thickness for

Presented as Paper 2013-0186 at the 51st AIAA Aerospace Sciences Meeting Including the New Horizons Forum and Aerospace Exposition, Grapevine, TX, 6–10 January 2013; received 21 March 2013; revision received 8 August 2013; accepted for publication 8 August 2013; published online 20 February 2014. Copyright © 2013 by the authors. Published by the American Institute of Aeronautics and Astronautics, Inc., with permission. Copies of this paper may be made for personal or internal use, on condition that the copier pay the \$10.00 per-copy fee to the Copyright Clearance Center, Inc., 222 Rosewood Drive, Danvers, MA 01923; include the code 1533-3876/14 and \$10.00 in correspondence with the CCC.

*Ph.D. Candidate, Dipartimento di Ingegneria Meccanica e Aerospaziale, Via Eudossiana 18; currently von Karman Institute for Fluid Dynamics, 1640 Rhode-Saint-Genèse, Belgium. Student Member AIAA.

†Assistant Professor, Dipartimento di Ingegneria Meccanica e Aerospaziale, Via Eudossiana 18. Member AIAA.

‡Senior Development Engineer. Senior Member AIAA.

§Associate Professor, Dipartimento di Ingegneria Meccanica e Aerospaziale, Via Eudossiana 18. Associate Fellow AIAA.

¶William R. T. Oakes Professor and Chair, School of Aerospace Engineering. Fellow AIAA.

adequate thermal protection requires taking into account the interactions between the ablative material and its operating environment. Furthermore, erosion of the nozzle throat reduces the nozzle area ratio and consequently decreases the overall engine performance. Generally, to determine the ablative material thickness needed to protect the structural components of the nozzle, and to quantify the nozzle erosion rate, firing tests on full-scale motors are conducted. These tests, however, are costly both in time and expense. An efficient and more economical approach would be to couple the full-scale experiments with modeling studies.

The overall description of nozzle erosion phenomena has been the subject of many investigations, and preliminary studies go back to the early 1960s [3,4]. A much more detailed and comprehensive model was later developed by Kuo and Keswani [5,6] to study the thermochemical erosion of carbon-carbon (C-C) nozzles, accounting for both diffusion and chemical kinetics effects. This model, based on the combined inviscid core flow and viscous boundary-layer flow equations, has recently been updated by Acharya and Kuo [7,8]. Recent studies based on full Navier-Stokes approaches have been carried out independently by different research groups for carbon-carbon and graphite nozzles [9–13] as well as for carbon-phenolic nozzles [14,15] and for refractory metal nozzle inserts [16].

The thermochemical erosion of carbonaceous materials (e.g., graphite, carbon-carbon, and carbon-phenolic) is caused by the endothermic heterogeneous reactions that occur between the oxidizing species (H_2O , CO_2 , and OH) and the heated nozzle material. These oxidizing species diffuse across the boundary layer toward the surface, forming a concentration boundary layer. The nozzle recession rate can be influenced by both the chemical kinetics of the heterogeneous reactions at the surface and the diffusion of the oxidizing species across the boundary layer. These mechanisms can be affected, in turn, by the morphological, thermal, and chemical characteristics of both the flow and the TPS material. Surface roughening due to erosion, for example, can affect the subsequent erosion rate because of its effect on the turbulent boundary layer, modifying the mass and energy transfers toward the nozzle wall. Increased roughness can also increase the gas-solid interaction surface, generating higher availability of reacting sites [17,18]. Unfortunately, a comprehensive treatment of this important aspect of ablation involves such a wide range of different scales that it is impractical to model the whole ablative nozzle response.

Recently, a validated theoretical and numerical framework [9] was used to study separately the effects of combustion gas radiation and surface roughness on the erosion of carbon-based materials in solid rocket motors loaded with nonmetallized ammonium perchlorate-hydroxyl-terminated polybutadiene (AP/HTPB) composite propellants [19]. In that work, the two layer $k-\epsilon$ turbulence model was modified to account for surface roughness effects, and average values of gas-phase emissivity were considered to study radiation effects. The numerical simulations showed that the wall radiative heat transfer and enhanced near-wall turbulence due to surface roughness could have a complementary effect on the erosion of the carbon-carbon surface in a nonmetallized solid-propellant rocket environment. Results obtained in the nonmetallized environment cannot be extrapolated to propellants with significant amount of aluminum. Roughness effects could be different in the case of metallized propellant because of lower erosion rates than nonmetallized propellant. Radiation effects can also be quite different. It can be expected that radiation effects are more important in the case of aluminized solid propellant, because of the enhanced combustion products temperature and of the presence of alumina particles. Therefore, the common assumption that in typical operating conditions the net radiative heat flux is an order of magnitude lower than its convective counterpart may not hold. Consequently, radiation effects may not be neglected as is commonly done [5,7,12,16], especially if the interest is focused not only on the throat region but also on the converging part of the nozzle.

In this work, based on the results obtained for nonmetallized propellants in [19], radiation and roughness effects are introduced into a previously validated model [11–15] to study the thermochemical erosion of graphite nozzles in solid rocket motors loaded

with either metallized or nonmetallized AP/HTPB composite propellants. Moreover, the effects of roughness and radiation are analyzed both separately, as done in [19], and jointly. The general model includes the Reynolds averaged Navier-Stokes (RANS) equations for the gas phase, the energy equation for the solid phase (nozzle material), and the boundary conditions at the gas-solid interface. Surface roughness is modeled according to the equivalent sand grain approach, which, in a RANS solver, can be included via different turbulence models. For instance, a two-equation ($k-\epsilon$) model is used in [19] and a one-equation model (Spalart-Allmaras) is considered in the present study. The selection of the latter turbulence model is based on its simplicity and reliability in the study of attached boundary layers and on its straightforward extension to rough walls [20]. The radiation effect is included through simplified models based on its dependence on bulk gas temperature, wall temperature, and aluminum content.

II. Theoretical Formulation

A. Gas-Phase Modeling

The gas phase consists of the multicomponent mixture arising from the combustion products of the selected propellants. The governing equations for the gas phase are the reacting turbulent RANS equations [21]:

$$\begin{cases} \frac{\partial(\rho y_i)}{\partial t} + \nabla \cdot (\rho \mathbf{v} y_i) + \nabla \cdot \mathbf{j}_i = \dot{w}_i, & i = 1, \dots, N_s \\ \frac{\partial \rho}{\partial t} + \nabla \cdot (\rho \mathbf{v}) = 0 \\ \frac{\partial(\rho \mathbf{v})}{\partial t} + \nabla \cdot (\rho \mathbf{v} \mathbf{v}) - \nabla \cdot \mathbb{S} = 0 \\ \frac{\partial(\rho e_0)}{\partial t} + \nabla \cdot (\rho e_0 \mathbf{v}) = \nabla \cdot (\mathbf{v} \cdot \mathbb{S}) - \nabla \cdot \dot{\mathbf{q}} \end{cases} \quad (1)$$

The term \mathbb{S} is the stress tensor, split into the contributions of pressure forces and viscous stresses (\mathbb{T}); the term $\dot{\mathbf{q}}$ is the heat flux vector; and the term \dot{w}_i is the source term due to chemical reactions:

$$\begin{aligned} \mathbb{S} &= -p\mathbb{I} + \mathbb{T} \\ \mathbb{T} &= -\frac{2}{3}\mu(\nabla \cdot \mathbf{v})\mathbb{I} + \mu[\nabla \mathbf{v} + (\nabla \mathbf{v})^T] \\ \dot{\mathbf{q}} &= -k\nabla T + \sum_{i=1}^{N_s} h_i \mathbf{j}_i \end{aligned} \quad (2)$$

where \mathbb{I} is the unit tensor. The diffusive mass flux of the i th species \mathbf{j}_i can be expressed using the approximation of Fick's law:

$$\mathbf{j}_i = -\rho D_{im} \nabla y_i \quad (3)$$

The thermodynamic properties of individual species are approximated by seventh-order polynomials of temperature, whereas the transport properties are approximated by fourth-order polynomials [22]. Mixture properties for conductivity and viscosity are derived from Wilke's rule. The diffusion model is based on the effective diffusion coefficients defined as [23]

$$D_{im} = (1 - x_i) / \sum_{j \neq i}^{N_s} x_j / D_{ij} \quad (4)$$

Equation (4) does not guarantee that the diffusive fluxes would sum to zero. Equation (3) is hence modified to ensure that the mass fluxes sum to zero by distributing the residual according to the species mass fraction [24]. The diffusive mass fluxes, first calculated by Eq. (3), are corrected by

$$\mathbf{j}_{i,\text{corr}} = \mathbf{j}_i - y_i \sum_{i=1}^{N_s} \mathbf{j}_i \quad (5)$$

For the present study, the gas-phase reactions are considered to have a negligible effect on the recession process (frozen flow in the gas phase). This assumption is justified by chemical equilibrium calculations [22] showing little effect on the boundary-layer concentrations of oxidizing species in the nozzle sections of interest.

B. Ablative Boundary Condition

Based on the assumption that no material is being removed in the condensed phase (solid or liquid), the general surface balances for a chemically reacting ablating surface are

$$\rho D_{im} \frac{\partial y_i}{\partial \eta} \Big|_w + \dot{\omega}_i = \dot{m} y_{i_w}, \quad i = 1, \dots, N_s \quad (6)$$

$$k \frac{\partial T}{\partial \eta} \Big|_w + \sum_{i=1}^{N_s} h_{i_w} \rho D_{im} \frac{\partial y_i}{\partial \eta} \Big|_w + \dot{m} h_{s_w} + \dot{q}_{\text{radin}} = \dot{m} h_w + \dot{q}_{\text{radout}} + \dot{q}_{\text{cond}} \quad (7)$$

In Eq. (6), which is the surface mass balance for the i th species, the terms on the left-hand side are, respectively, the mass fluxes of species i entering the surface due to diffusion and the heterogeneous surface reactions between the boundary-layer gases and the surface carbon, whereas the term on the right-hand side is the mass flux of species i leaving the surface due to surface ablation.

Equation (7) is the surface energy balance. The terms on the left-hand side are, respectively, the energy fluxes entering the surface due to conduction from gas, diffusion, surface carbon mass flux, and radiation from the combustion gas, whereas the terms of the right-hand side are, respectively, the energy fluxes leaving the surface due to surface ablation, reradiation from the wall, and conduction in the solid phase. The heat conduction process in the nozzle is treated as one dimensional. When the steady-state condition of a planar surface is considered, a closed solution of the in-depth energy balance can be achieved from its integration between the hot (front) surface and the cold (back) surface of the material. Therefore, the steady-state solid conduction term reads

$$\dot{q}_{\text{cond}}^{\text{SS}} = \dot{m}(h_{s_w} - h_{s_0}) \quad (8)$$

where h_{s_w} and h_{s_0} represent the enthalpy of the solid carbon at the wall temperature and at the initial temperature, respectively.

The heterogeneous gas-surface chemical reactions are described by a semiglobal heterogeneous reaction mechanism for graphite oxidation [25,26]. A subset of this reaction mechanism, consisting of three reactions (excluding erosion contributions from species O and O₂, whose concentrations are negligibly small in solid-propellant combustion products), has recently been validated for graphite nozzle erosion in solid rocket motors [7,9,12,13].

With this mechanism, the rate of consumption of carbon by the generic oxidizing species i (which can be H₂O, CO₂, or OH) can be expressed as

$$\dot{m}_i = \underbrace{p_i^n}_{\Phi_i} \cdot \underbrace{A_i T_w^b \exp(-E_i/RT_w)}_{\Psi_i} \quad (9)$$

where p_i is the partial pressure of oxidizing species i , T_w is the wall temperature, and n is the overall order of the heterogeneous reaction. The terms A_i and E_i are the preexponential factor and the activation energy of the heterogeneous reaction, respectively. The kinetic parameters of Eq. (9) for the three reactions are taken from [26] and reported in Table 1. Reaction rates are assumed to be independent of each other according to results and discussions presented in [7,9,13,25,26]. The two terms labeled as Φ_i and Ψ_i in Eq. (9) are the partial pressure term (which is a function of the reaction order n) and the specific rate constant of the reaction, respectively. The rate of production/consumption of the generic gas-phase species i at the nozzle surface, $\dot{\omega}_i$, in Eq. (6), can be easily derived from the rate of

Table 1 Kinetic data for heterogeneous surface reactions [26]

Surface reaction	A_i	E_i , kJ/mol	b	n
$C_s + H_2O \rightarrow CO + H_2$	4.80×10^5	288.0	0.0	0.5
$C_s + CO_2 \rightarrow 2CO$	9.00×10^3	285.0	0.0	0.5
$C_s + OH \rightarrow CO + H$	3.61×10^2	0.0	-0.5	1.0

erosion of carbon by the generic oxidizing species, Eq. (9), and the mass balance available once the species molecular weights and the stoichiometry of the surface reactions are known. Finally, the total erosion rate of carbon due to the surface heterogeneous reactions can be evaluated as

$$\dot{m} = \sum_{i=1}^{N_s} \dot{\omega}_i = \dot{m}_{H_2O} + \dot{m}_{CO_2} + \dot{m}_{OH} = (\rho v)_w = \rho_s \dot{s} \quad (10)$$

C. Extension of the Spalart–Allmaras Turbulence Model to Account for Surface Roughness

A correction of the Spalart–Allmaras turbulence model is implemented to account for the effect of surface roughness [20,27]. This modification is based on the “equivalent sand grain approach,” which, by means of empirical correlations (i.e., Dirling [28]), associates the actual surface roughness to that of a sand grain roughened wall. The effects of roughness were extensively investigated by Nikuradse in the 1940s [29]; his experimental analyses showed a clear relationship between the normalized velocity profile shifting, Δu^+ , and the normalized roughness: $h_{\text{eq}}^+ = h_{\text{eq}} u_\tau / \nu$. This velocity profile shifting can be evaluated once the value of the equivalent sand grain roughness is known.

The basic equation of the Spalart–Allmaras model reads [30]

$$\frac{D\tilde{\nu}}{Dt} = c_{b1} \tilde{S} \tilde{\nu} + \frac{1}{\sigma} \{ \nabla \cdot [(\nu + \tilde{\nu}) \nabla \tilde{\nu}] + c_{b2} (\nabla \tilde{\nu})^2 \} - c_{w1} f_w \left(\frac{\tilde{\nu}}{d} \right)^2 \quad (11)$$

where the terms of production, diffusion, and destruction of the turbulent viscosity $\tilde{\nu} = \nu_\tau / f_{v1}$ are on the right-hand side. The “Boeing extension” of the Spalart–Allmaras model presented in [20] was developed to mimic the normalized velocity (u^+) shifting, observed experimentally in the logarithmic region and the outer region of the boundary layer, in the case of flow over rough surfaces. This is achieved by increasing the turbulent eddy viscosity in the wall region. In order to take into account the roughness effect, distance term d is modified as

$$d = d_{\text{min}} + d' \quad (12)$$

where d_{min} is the distance from the equivalent smooth wall (assumed to be located part-way up the roughness) and $d' = d'(h_{\text{eq}})$. The value of $d'(h_{\text{eq}})$, derived from the Nikuradse [29] experiments, is

$$d' = \exp(-8.5\kappa) h_{\text{eq}} \quad (13)$$

where $\kappa = 0.41$ is the von Kármán constant. Moreover, in order to obtain accurate results when dealing with small roughness, the variable $\chi = \tilde{\nu} / \nu$ is redefined as follows:

$$\chi = \frac{\tilde{\nu}}{\nu} + c_{R1} \frac{h_{\text{eq}}}{d} \quad (14)$$

where $c_{R1} = 0.5$. Therefore, to retain the \tilde{S} expression, defined as

$$\tilde{S} = S + \frac{\tilde{\nu}}{\kappa^2 d^2} f_{v2}$$

the definition of $f_{v2} = 1 - [\chi/(1 + \chi f_{v1})]$ is modified as follows:

$$f_{v2} = 1 - \frac{\chi - c_{R1} h_{eq}/d}{1 + f_{v1}(\chi - c_{R1} h_{eq}/d)} = 1 - \frac{\tilde{\nu}}{\nu + \tilde{\nu} f_{v1}} \quad (15)$$

Finally, the $\tilde{\nu} = 0$ wall boundary condition is replaced by

$$\frac{\partial \tilde{\nu}}{\partial \eta} = \frac{\tilde{\nu}}{d} = \frac{\tilde{\nu}}{0.03 h_{eq}} \quad (16)$$

This modified model was extensively tested and found to produce results comparable to those obtained by the best-tested roughness models [20].

The present surface roughness treatment has been validated against the results obtained by Aupoix and Spalart [20] for a specific test case involving air flowing at 58 m/s over a heated flat plate. The test case reproduces the experimental data obtained by Hosni et al. [31,32] made over electrically heated flat plates of different roughnesses. Figure 1a shows the normalized velocity profile obtained using the implemented modification. The shifting of the velocity profiles in the case of wall roughness is evident, and the result for the highest roughness level agrees reasonably well with that reported in [20]. Figure 1b shows the calculated skin friction coefficient as well as the Stanton number along the length of the plate, together with those reported in [20].

D. Gas and Surface Radiation

Radiative heat flux can affect the nozzle erosion behavior, especially in the converging part of the nozzle, where the convective heat flux is lower than in the throat region. This effect was analyzed in [19] for a nonmetallized propellant; a 4.5–13.6% reduction of the erosion rate was found when both gas and wall radiation were considered, depending on the level of gas emissivity, as opposed to the case without any contribution from radiation. It was further noted that, when dealing with aluminized propellants, the erosion rate could be higher than its counterpart without radiation. In fact, in aluminized propellants, the radiative heat flux coming from the two-phase gas-particles mixture can represent a nonnegligible fraction of the heating [33]. To obtain a simple estimate of the particle radiation effect, two different simplified models have been considered for calculating the integral emissivity of the dispersed alumina particles. The first model derives from empirical specification of the integral emissivity near the nozzle throat of a small-scale solid rocket motor operating with metallized propellants [34]:

$$\dot{q}_{rad,in} = \alpha_s \underbrace{\left[1 - \exp\left(\frac{-3.972 n \rho_b r}{16}\right) \right]}_{\epsilon_g} \sigma T_b^4 \quad (17)$$

where ρ_b is the gas bulk density in kilograms per cubic meter, r is the local radius in meters, and n is the percentage (by mass) of aluminum content in the propellant. Equation (17) is based on experimental data of radiation obtained on a small-scale solid rocket motor, where emission measurements were made from the optical path across the throat diameter (3.18 cm).

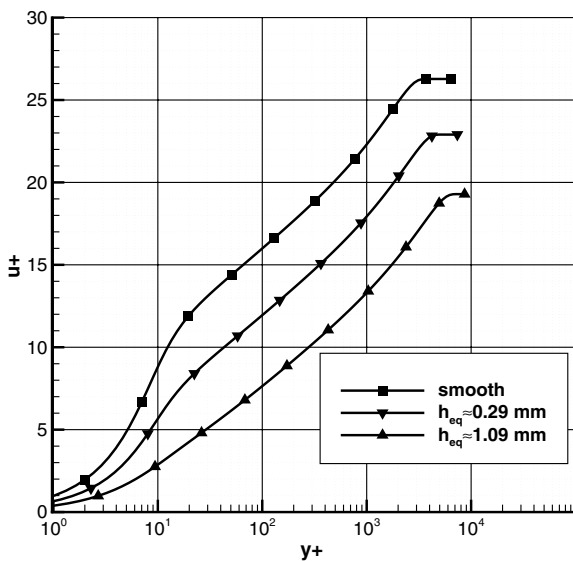
This model will be referred to as “model A.” Figure 2a shows the calculated integral emissivity as a function of the gas density using the local radius as a parameter. The strong sensitivity of the emissivity to local radius is evident; the emissivity-density dependence is almost linear for smaller radii.

The second model is taken from [35] and represents the limiting value of the integral hemispherical emissivity of an optically thick cloud of monodispersed alumina particles:

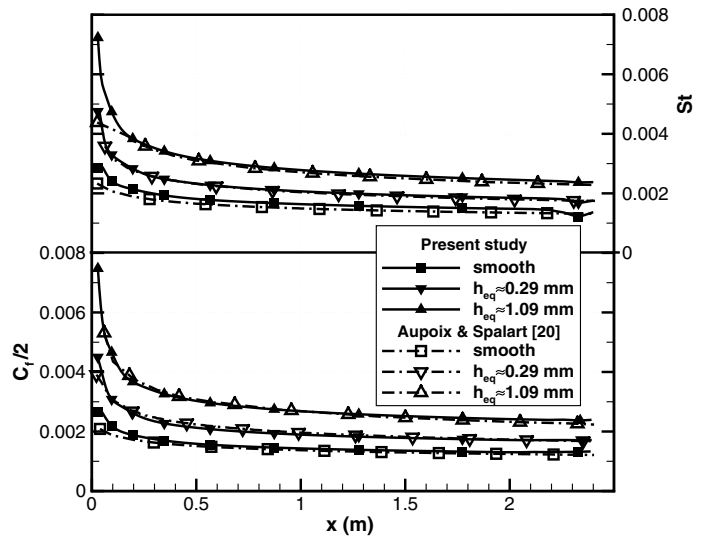
$$\dot{q}_{rad,in} = \alpha_s \underbrace{[0.17 + 0.22 \tilde{T}_b - (0.87 - 0.1 \tilde{T}_b) \exp(-0.22 \tilde{T}_b a)]}_{\epsilon_g} \sigma T_b^4 \quad (18)$$

where $\tilde{T}_b = T_b/1000$ is a reduced value of the bulk temperature (particles and gas are considered in thermal equilibrium), expressed in degrees Kelvin, and a represents the particle radius in micrometers. This second model will be referred to as “model B.” It should be noted that, although Eq. (18) was derived for the combustion chamber, it has been employed for the nozzle flow. Because the purpose of the present work is to estimate the influence of the radiative heat flux on nozzle erosion, rather than the accurate evaluation of the radiation inside the nozzle, these two simplified models have been considered suitable for the analysis. Figure 2b shows the emissivity-temperature dependence using the particle radius as the parameter. Interestingly, for higher values of particle radii the particle size has a very low influence on the calculated integral emissivity.

According to [35], for an optically thick volume of typical combustion products, the integral emissivity calculated considering only the condensed phase is more than 99% of that calculated including the radiation contribution of the gaseous products. For this reason, the gas-phase contribution has been neglected in the evaluation of the integral emissivity of the combustion products. Concerning the wall emissivity, a single constant value is considered as representative of



a) Normalized velocity



b) Skin friction coefficient and Stanton number

Fig. 1 Normalized velocity profile, skin friction coefficient, and Stanton number for smooth and rough walls.

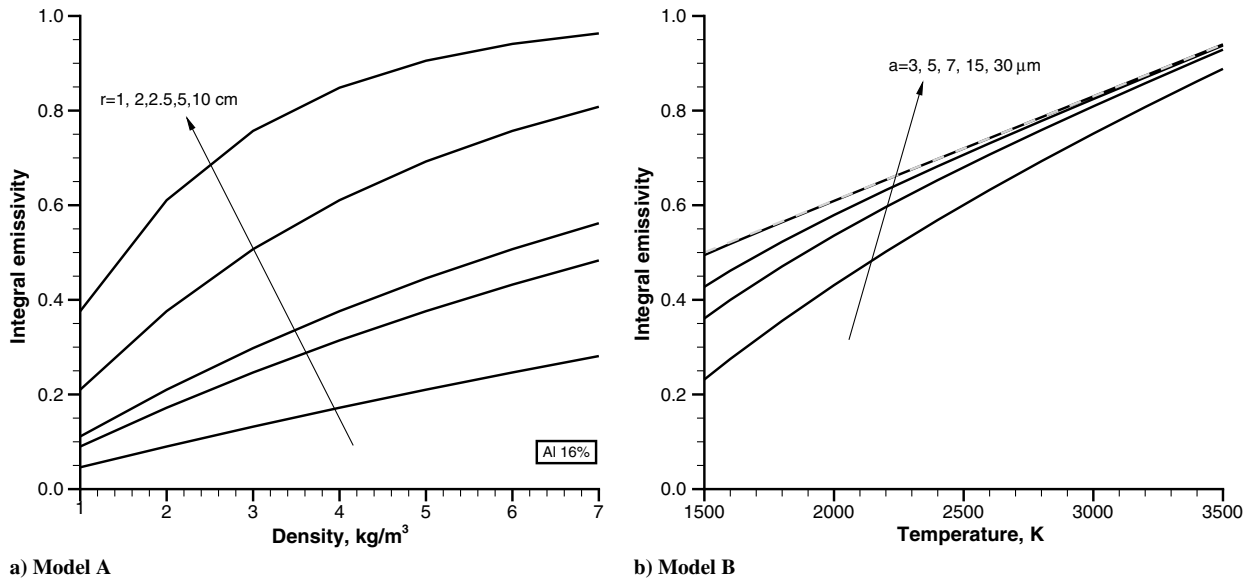


Fig. 2 Integral particle emissivity evaluated with different models.

the nozzle wall. Hence, wall reradiation varies only due to the change in wall temperature dictated by

$$\dot{q}_{\text{rad,out}} = \sigma \epsilon_s T_w^4 \quad (19)$$

and the net radiative heat flux can be evaluated as follows:

$$\dot{q}_{\text{rad}} = \dot{q}_{\text{rad,in}} - \dot{q}_{\text{rad,out}} \quad (20)$$

III. Test Case Input Data

In this study, both nonmetallized and metallized AP/HTPB composite propellants have been considered to study the effects of surface roughness and radiation on graphite nozzle erosion. These propellants are those adopted in the experimental work by Evans et al. [36]. The equilibrium compositions and the chamber conditions are shown in Table 2. The graphite nozzle ($\rho_s = 1.92 \text{ g/cm}^3$) is that of the motor described in [37], having a throat diameter of 2.0 in. As far as reradiation is concerned, a single emissivity value of $\epsilon_s = 0.9$ has been used for the graphite surface [38]. The surface has been assumed to be gray, which permits the use of the same value for wall emissivity and absorptivity ($\epsilon_s = \alpha_s$). When required [see Eq. (18)], a radius of $10 \mu\text{m}$ has been considered for the alumina particles [39]. The particle size could be higher due to particle agglomeration. The emissivity value, however, has a low sensitivity to the particle radius in the temperature range of interest (see Fig. 2b). For this reason, the selected particle size can be considered suitable for the analysis.

Several values of equivalent sand grain roughness have been considered in the analysis. Experimental tests of graphite-nozzle turbulent flows show that a typical “scaloped” surface is established,

with length scales on the order of 1 mm [40,41]. Numerical analyses performed in [17,18] show that the steadiness of this surface morphology is ensured, allowing the use of a single constant surface roughness value, once the steady state has been reached. The Dirling correlation [28] for calculating the equivalent sand grain roughness gives values in the range of 5–50 μm . The values are in good agreement with the ones used in [19] and observed in nozzle postfiring data analyses [42].

IV. Results

In the present work, following the analysis performed in [19], a systematic study of both the separate and combined influence of surface roughness and radiation on erosion behavior has been performed.

A. Effect of Roughness

The first part of the analysis focuses on the effect of surface roughness on the nozzle erosion rate for both metallized and nonmetallized propellants. Figure 3 shows the calculated erosion rate profiles for both propellants. Two equivalent sand grain roughnesses have been considered: 10 and 50 μm . It should be noted that the first few points close to the nozzle entrance should not be considered quantitatively accurate due to the undeveloped boundary layer. Therefore, the plotted quantities are displayed starting about 1 mm downstream from the nozzle entrance for all the presented results. The effect of the surface roughness is evident, especially in the throat region. The erosion rate is enhanced, with respect to the baseline case (smooth wall), in the converging part of the nozzle. The roughness effect gradually enhances the erosion rate, as compared with baseline, up to a point slightly upstream of the throat. Then, the difference in the erosion rate level starts decreasing and the influence of the surface roughness falls below 10% of its peak variation at an expansion ratio of approximately 2 (for $h_{\text{eq}} = 10 \mu\text{m}$) and 2.5 (for $h_{\text{eq}} = 50 \mu\text{m}$) for both propellants.

It should be noted that the erosion regime is different for the two propellants, kinetic limited for the nonmetallized and diffusion limited for the metallized, due to the higher chamber temperature and lower oxidizing species content of the latter [12]. This is confirmed by the plots in Fig. 4, which show the total wall mass fraction of the three oxidizing species. When the wall mass fraction of the oxidizing species goes to zero, it means that the reaction kinetics are faster than the diffusive process, as the surface reactions are capable of consuming instantaneously all the reactants arriving at the reaction sites. Therefore, the process that limits the graphite oxidation rate is the diffusion of the reactants toward the surface. For the metallized

Table 2 Chamber conditions and species mass fractions for the two propellants

Propellant	Nonmetallized	Metallized
p_c , bar	56	56
T_c , K	3000	3512
Al_2O_3	—	0.33
CO	0.10	0.22
CO_2	0.21	0.02
H_2	0.01	0.02
HCl	0.29	0.24
H_2O	0.28	0.08
N_2	0.11	0.08
OH	—	0.01

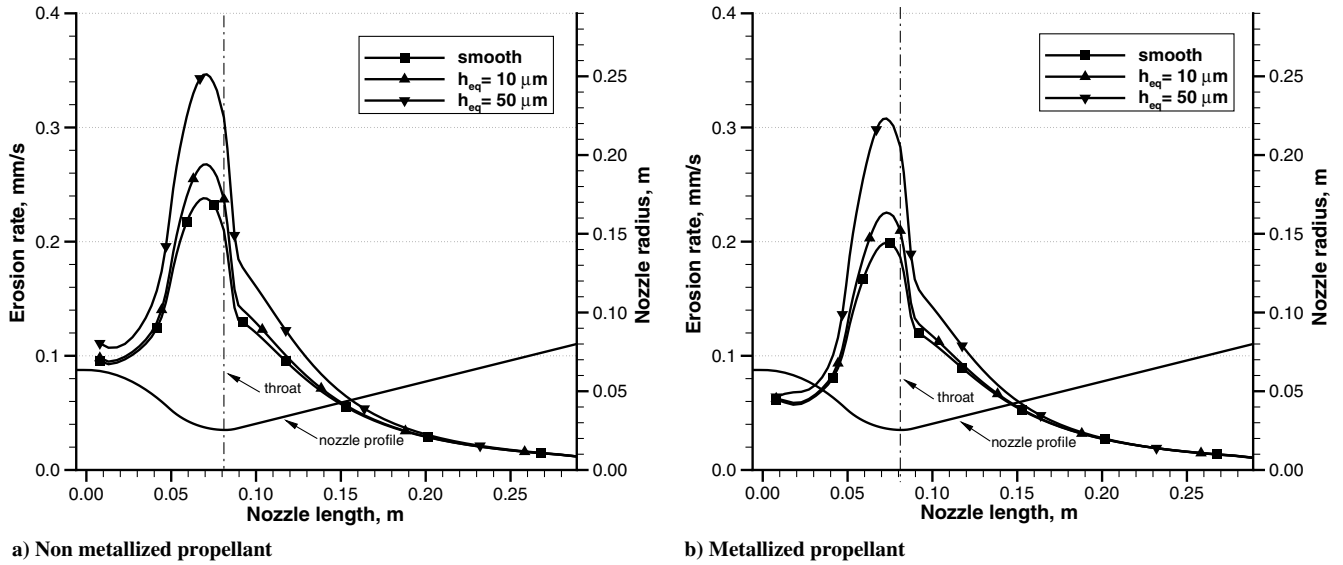


Fig. 3 Erosion rate for different surface roughness and different propellants along the nozzle length.

propellant, almost 95% by mass of the exhaust gas oxidizing species is consumed at the surface, whereas only 30% is consumed in the case of nonmetallized propellant, denoting a kinetic-limited erosion regime for the latter.

The wall temperature profiles are plotted in Fig. 5. In the rough wall case, the temperature increases in the throat region and in the diverging part of the nozzle with respect to the baseline case for both propellants. Nevertheless, the temperature profiles are qualitatively different for the two propellants, due to the different erosion regimes, which generate a different coupling between the mass and energy balances at the nozzle interface. In the diffusion-limited regime, the erosion rate can affect the surface temperature through the surface energy balance, but the change in surface temperature can only marginally affect the erosion rate. In the kinetic-limited regime, on the other hand, both the erosion rate and the surface temperature can affect each other. The temperature profiles in the case of non-metallized propellant qualitatively mimic the erosion-rate profiles, for both smooth and rough walls. For the metallized propellant, however, the rough wall causes the temperature to drop below the baseline value in the converging section. Slightly upstream of the throat, the rough wall temperature profiles cross the baseline value and the differences between the temperature profiles hold along the entire divergent section. The erosion rate, on the other hand, is always higher in the case of the rough wall for the metallized propellant

(Fig. 3b) despite an initial reduction of the wall temperature (Fig. 5b). The change of slope immediately after the throat is a consequence of the nozzle geometry. The diverging part of the nozzle is in fact conical, and the change in the curvature of the profile downstream causes the abrupt variation of the flow quantities.

Focusing on the throat section, the local values of the convective heat flux, erosion rate, wall temperature, and H_2O contribution to the erosion rate are plotted in Fig. 6 for different values of the equivalent sand grain roughness (h_{eq}). The nondimensional values are normalized with respect to the baseline case (smooth wall). As seen, the differences in the convective heat flux and erosion rate between the two propellants are undetectable for h_{eq} values up to $20 \mu m$. For the higher values of h_{eq} , however, the metallized propellant shows a higher sensitivity to the roughness level. The erosion rate and the convective heat flux show practically the same trends. Despite the strong variation in the erosion rate, the wall temperature variation for the metallized propellant is smaller than for the nonmetallized one. This behavior is attributed to the different erosion regimes for the two propellants. In Fig. 6d, the left-hand side of Eq. (9) is plotted, for H_2O , together with the two right-hand side contributions (Φ_i and Ψ_i). The Ψ_{H_2O} term has a higher influence on \dot{m}_{H_2O} for the nonmetallized propellant, confirming the dominant role of the wall temperature, typical of the kinetic-limited regime. For the metallized propellant, in contrast, the higher influence of the Φ_{H_2O} term is evident because of

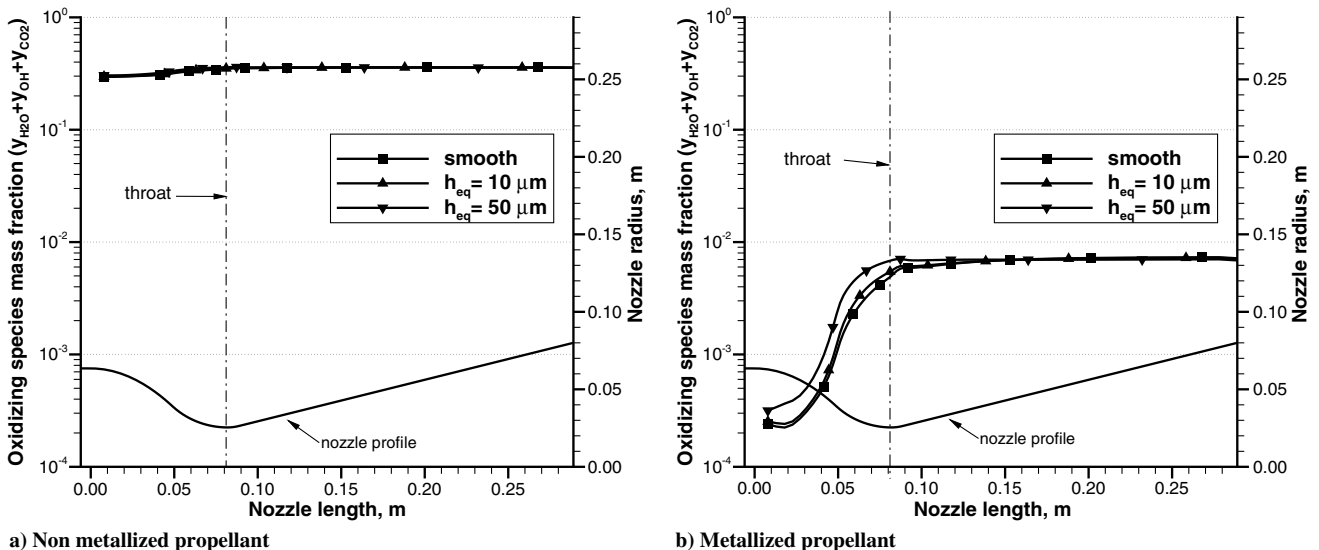


Fig. 4 Oxidizing species total wall mass fraction for different surface roughness and different propellants along the nozzle length.

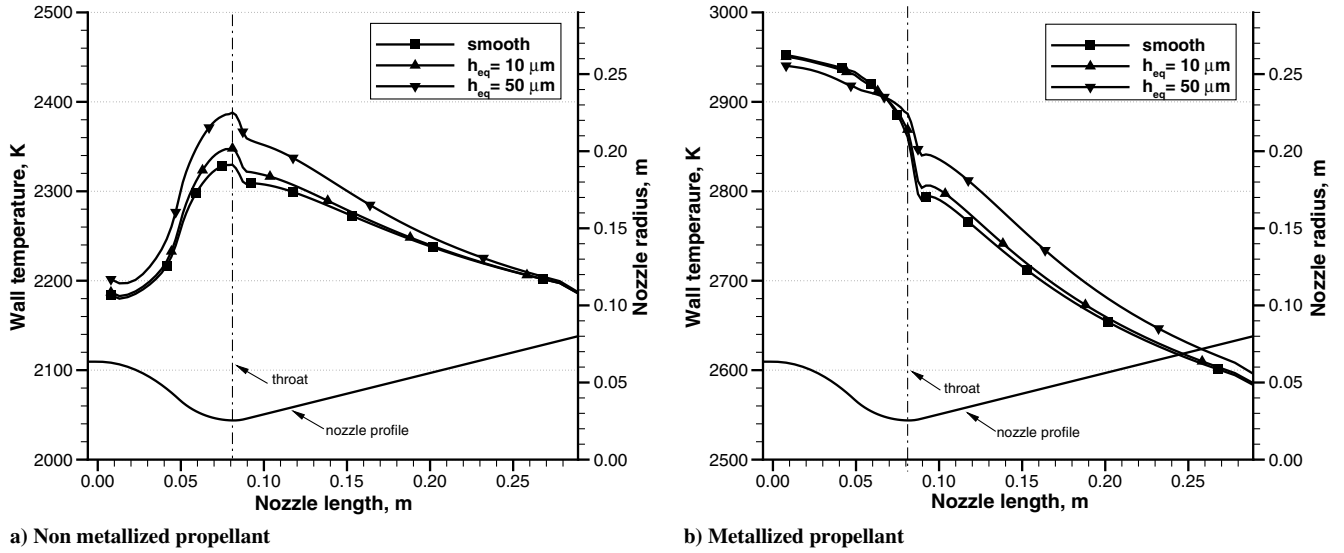
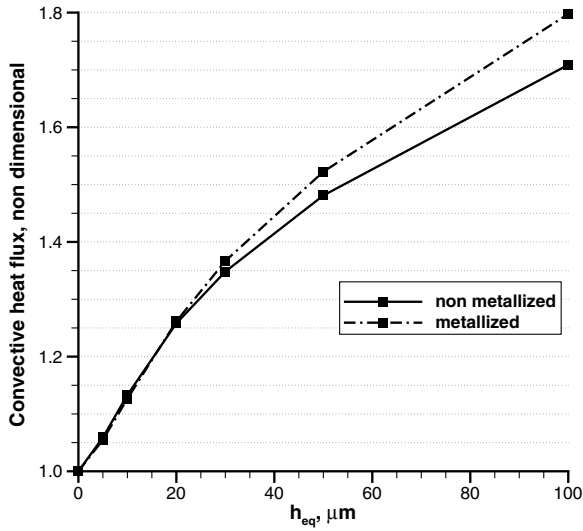
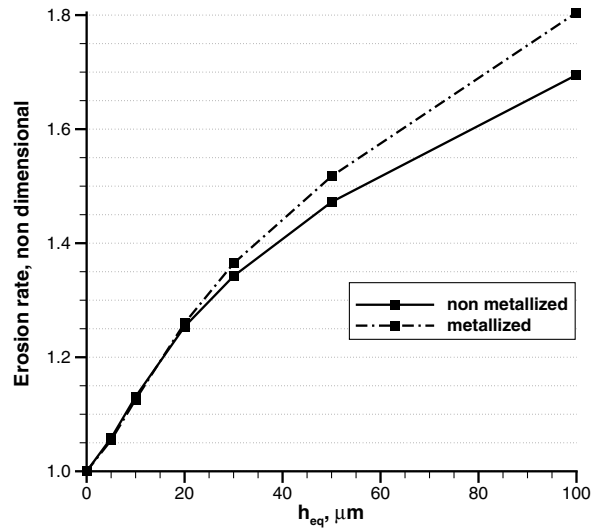


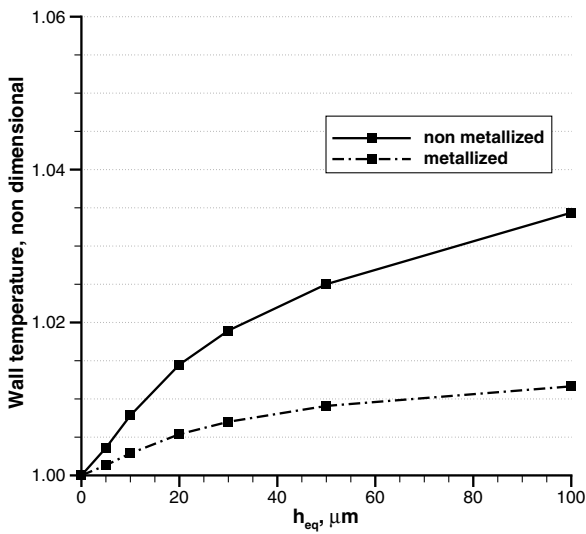
Fig. 5 Wall temperature for different surface roughness and different propellants along the nozzle length.



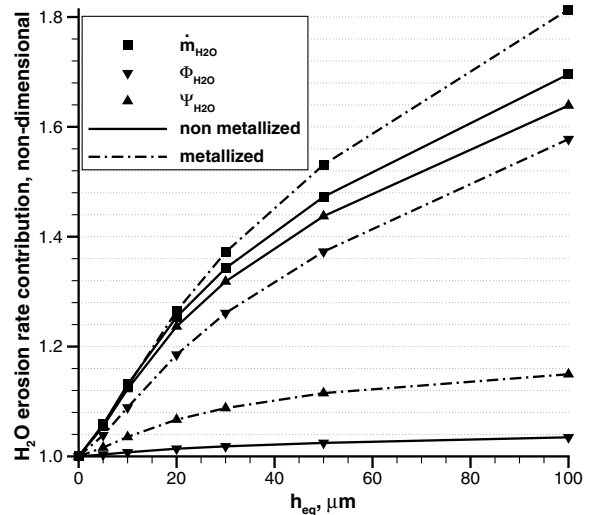
a) Convective heat flux



b) Erosion rate



c) Wall temperature



d) Single species (H_2O) total and decomposed non dimensional contributions to the erosion rate [terms \dot{m}_i , Φ_i and Ψ_i in Eq. (9)]

Fig. 6 Nondimensional plots of different throat quantities (normalized with respect to the smooth-wall value) as a function of the equivalent sand grain roughness for the two propellants.

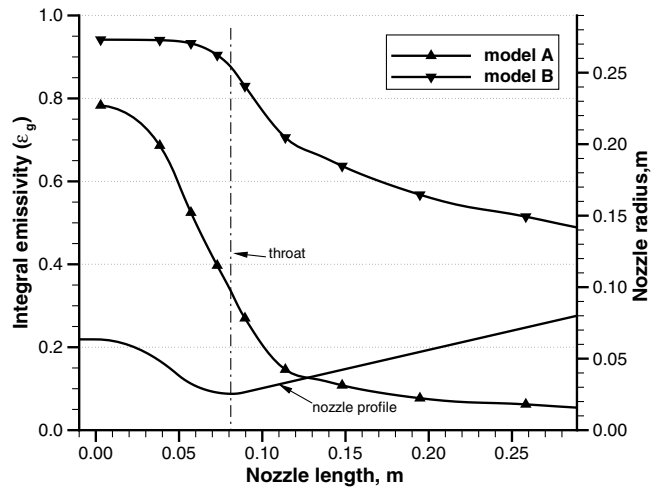
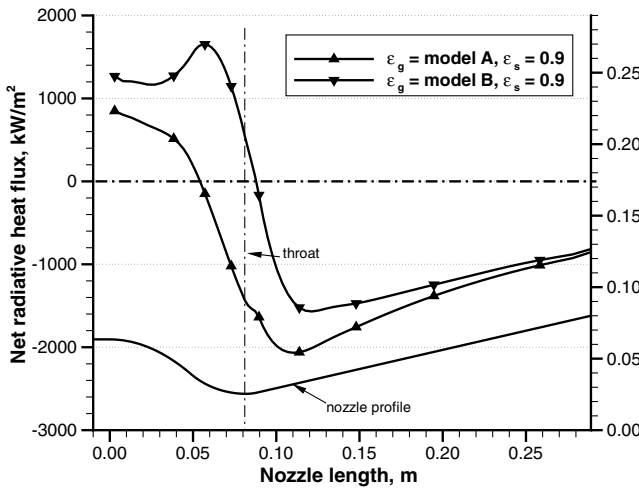
its diffusion-limited regime and the change in wall temperature only marginally affects the erosion mass flux. It is interesting to note that, although the driving mechanisms are different, the erosion rate increase with the equivalent sand grain roughness is qualitatively and quantitatively similar for both propellants and shows a cubiclike behavior.

B. Effect of Radiation

The second analysis evaluates the influence of the radiative heat flux on the nozzle erosion rate for both metallized and nonmetallized propellants. Radiative heat flux includes both the emission from the wall (reradiation) and the absorption by the wall due to gas/particle emission. The influence of radiation on the erosion rate for non-metallized propellants was studied in [19], showing the dominant role of surface reradiation, which counteracts the increased erosion due to roughness. A stronger effect can be therefore expected in the case of metallized propellants, due to the high emissivity of condensed alumina particles in the flow. Thus, the metallized propellant is analyzed first. The calculated net radiative heat fluxes are shown in Fig. 7, along with integral particle emissivity. The two different integral particle emissivities (Fig. 7b), calculated using simplified models A and B described previously, lead to different profiles of the net radiative wall heat flux (Fig. 7a). As expected, due to the high emissivity coupled with the high bulk temperature of the flow, the net radiative heat flux is positive (entering the wall) in the converging part of the nozzle. In the near-throat region, the reradiation from the

nozzle wall overcomes the incoming radiative heat flux and the net radiative heat flux becomes negative (leaving the wall). The reduction of the particle emissivity along the nozzle is more evident in the case of model A, because of the drop in gas density. The higher emissivity value of model B causes a difference of about 2.0 MW/m² in the net radiative heat flux at the throat section, as seen in Fig. 7a.

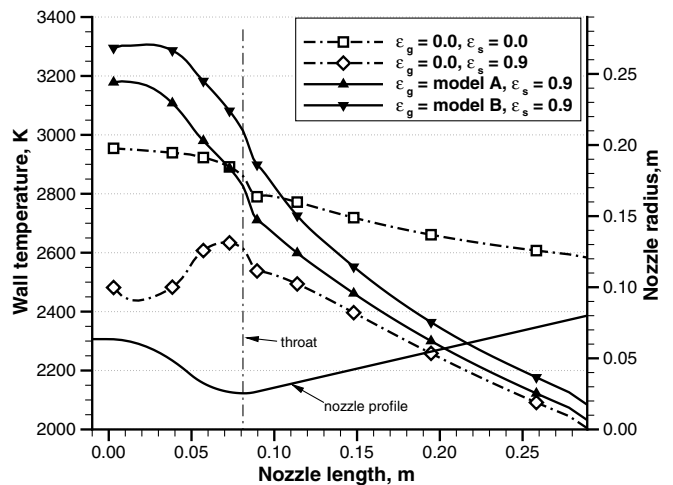
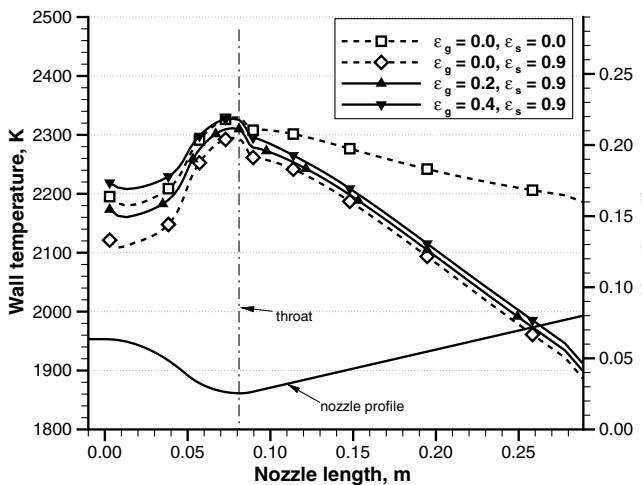
Figure 8 shows the calculated wall temperatures for both propellants. In addition to the baseline case without radiation, results with wall reradiation only and with both wall reradiation and gas/particle emissivity are shown. For the nonmetallized propellant, two different constant gas-phase emissivities ($\epsilon_g = 0.2$ and 0.4) are assumed, as in [19]. The emissivities of the individual gas-phase species at a given temperature and pressure were obtained from [43], where the average emissivity of gas phase is estimated in the range of 0.1–0.4. For the metallized propellant, both models A and B have been employed. The reduction of the wall temperature obtained when the wall reradiation is considered is quite significant, especially for the metallized propellant, which is characterized by a much higher wall temperature. Moreover, for the case including wall reradiation together with particle radiation (metallized propellant), the wall temperature profile is modified considerably (Fig. 8b). In particular, the wall temperature variation between the entrance and the exit sections is more than doubled. As far as the erosion rate is concerned, however, the influence of the radiative heat flux appears to be weaker in the case of the metallized propellant (Fig. 9b). The erosion rate decreases in the case of the nonmetallized propellant (Fig. 9a),



a) Net radiative heat flux

b) Integral emissivity

Fig. 7 Net radiative heat flux and integral emissivity of the combustion gas for the metallized propellant.



a) Non metallized propellant

b) Metallized propellant

Fig. 8 Wall temperature for different radiation models and different propellants along the nozzle length.

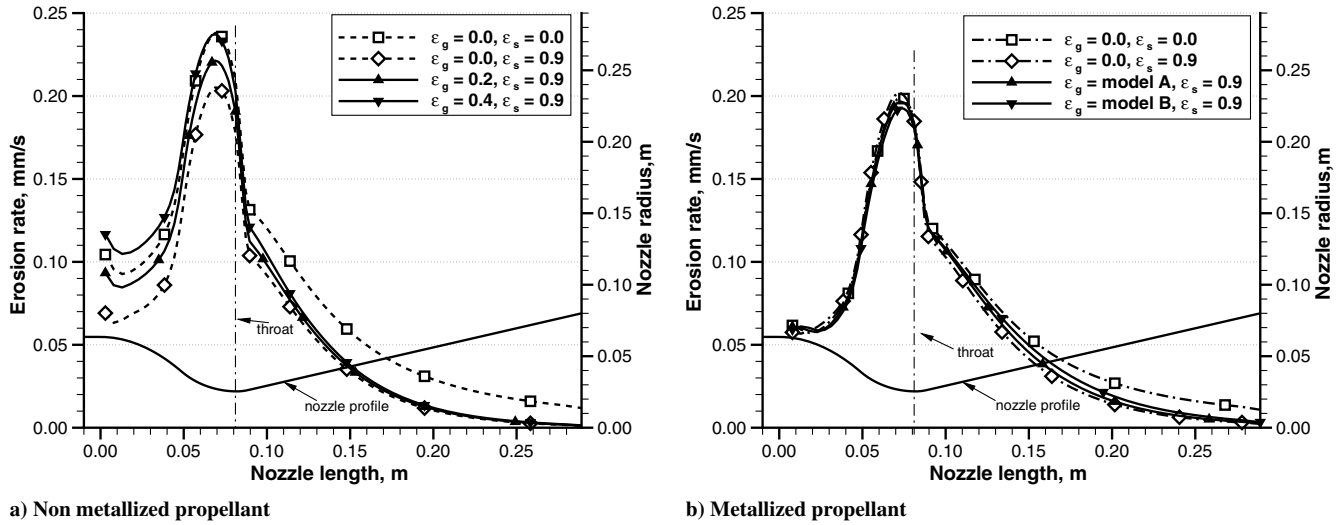


Fig. 9 Erosion rate profile for different radiation models and different propellants along the nozzle length.

confirming the results of [19]. In the case of metallized propellants, as a consequence of the diffusion-limited regime, the inclusion of the wall radiative heat transfer does not produce any significant variation of the erosion rate. The change in the wall temperature for metallized propellant still results in a diffusion-limited regime due to the high emissivity of the dispersed alumina particles. To further verify this behavior, a case was run with a constant value of integral particle emissivity along the nozzle, corresponding to the throat value obtained for each model (0.35 for model A and 0.88 for model B). Less than 3% difference in the throat erosion rate was obtained, implying that the influence on the erosion rate of using two significantly different constant integral emissivity values is negligible.

To characterize the throat erosion rate variation in the case of different gas/particle emissivities, the obtained results are compared against a reference throat erosion rate. This reference value, for each propellant, is the one obtained without considering any radiative heat transfer and has been used to nondimensionalize erosion rates in Figs. 10 and 11. In Fig. 10, the integral emissivity is used as the independent variable and the distribution of the nondimensional throat erosion rate is plotted for both propellants. For the non-metallized propellant (Fig. 10a), due to the kinetic-limited regime, the erosion rate is found to decrease due to radiation. When only wall reradiation is considered, the wall temperature shows the highest reduction (Fig. 8a), and the erosion rate is reduced by $\approx 15\%$ with

respect to the baseline value. When the gas phase emissivity is also included, the wall temperature reduction is lower and hence the erosion rate reduction becomes less significant.

For the metallized propellant (Fig. 10b), both models cause the throat erosion rate to decrease marginally with respect to the baseline value, and a maximum 3% reduction of the throat erosion rate is obtained when model B is used. This slight erosion rate reduction can be explained as an effect of the reduced diffusive mass flux caused by the higher wall temperature obtained when the particle radiation is considered (see Fig. 8b), especially for model B. The higher wall temperatures yield a less dense and thicker boundary layer leading to a lower diffusive mass flux and a lower diffusion-limited erosion rate. In the case of constant particle emissivities, if sufficiently low constant values of integral emissivity are considered, the wall reradiation contribution becomes dominant and the wall temperature can be sufficiently low to switch the erosion regime from diffusion limited to slightly kinetic limited, causing the erosion rate to increase with particle emissivity. The effect of change in the wall temperature on the erosion rate thus depends on the erosion regime. For the kinetic-limited regime, the erosion rate increases with wall temperature, whereas for the diffusion-limited regime it decreases due to the thickening of the boundary layer. At higher values of integral particle emissivities, the wall temperature is sufficiently high to ensure that the erosion is completely diffusion limited, so that any effect induced

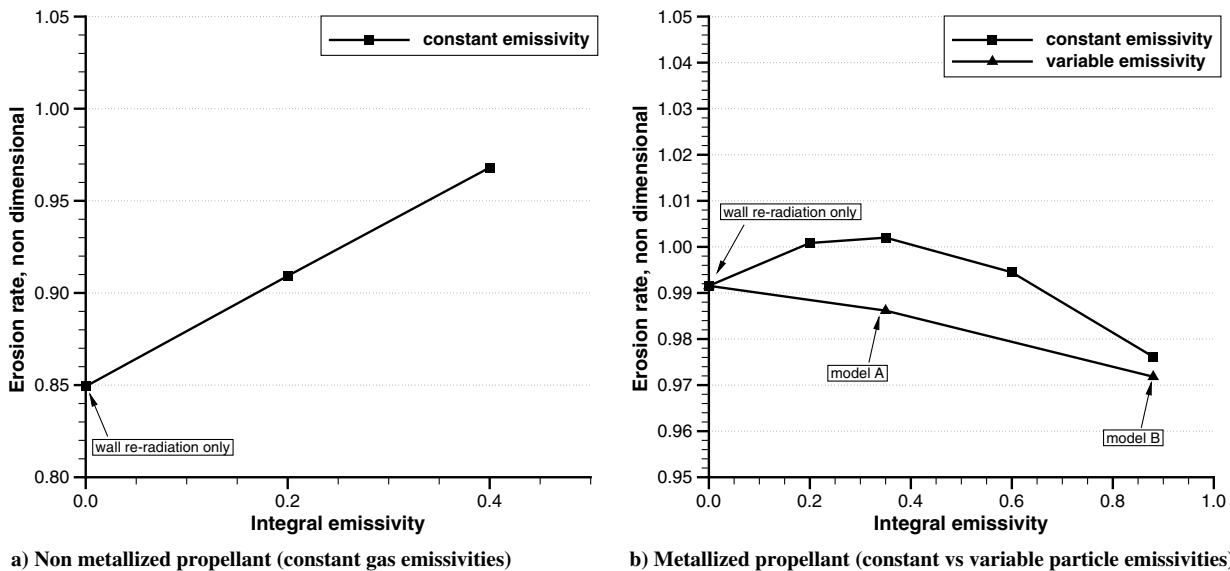


Fig. 10 Nondimensional throat erosion rate in the case of constant wall emissivity ($\epsilon_s = 0.9$) and different gas/particle emissivities for metallized and nonmetallized propellant.

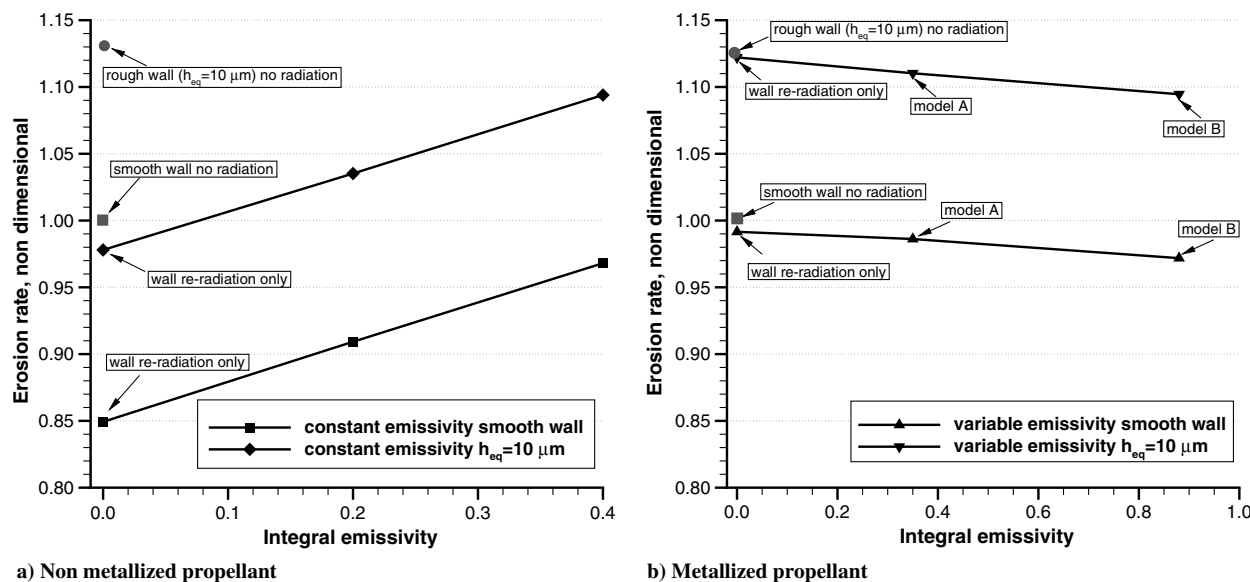


Fig. 11 Nondimensional throat erosion rate in the case of constant wall emissivity ($\epsilon_s = 0.9$) and constant/variable emissivities for both smooth and rough walls (metallized and nonmetallized propellant).

by the kinetic-limited regime disappears, and the obtained throat erosion rates are marginally lower than the baseline.

C. Combined Effect

Finally, the combined effects of particle radiation and wall roughness have been investigated. Figure 11 shows the nondimensional throat erosion rate as a function of the integral emissivity for both smooth and rough walls for the two propellants. The considered reference value is the throat erosion rate for a smooth wall, with no wall reradiation and no gas/particle radiation. The effect of radiation shows a similar trend on erosion rate, whether combined with surface roughness or considered alone. This trend can be noted by the similar slopes exhibited by the two curves in Figs. 11a and 11b. However, the integral gas/particle emissivity effect on erosion rate is opposite for the two propellants: erosion rate is increasing with integral emissivity in nonmetallized propellants, due to the kinetic-limited regime, whereas it is decreasing in metallized propellants, due to the diffusion-limited regime. Overall, it appears that the erosion rate is closer to the baseline value, particularly for nonmetallized propellants, when the combined effect is considered rather than surface roughness alone (circle symbol in Figs. 11a and 11b). It is also clear that surface roughness influences the erosion rate more than the radiation, especially for metallized propellants.

V. Conclusions

An analysis of surface roughness and gas/particle radiation effects on the thermochemical erosion of a solid rocket graphite nozzle has been carried out for both metallized and nonmetallized propellants. For typical values of surface roughness for graphite nozzles, a noticeable increase in the throat erosion rate is seen for both propellants. This increase is due primarily to the enhanced wall convective heat flux and species diffusive flux for a rough wall. As the two propellants generate two different erosion regimes, kinetic limited for the nonmetallized and diffusion limited for the metallized, the driving mechanisms that cause the change in erosion rate are different. In the case of the nonmetallized propellant, the augmented wall temperature enhances the heterogeneous reaction rates, causing a higher erosion rate. For the metallized propellant case, on the other hand, the stronger diffusion of the oxidizing species drives the erosion rate rise. It is interesting to note that, although the driving mechanisms are different, the erosion rate increase with the equivalent sand grain roughness is qualitatively and quantitatively similar for both propellants.

For nonmetallized propellant, the erosion rate has been found to decrease slightly due to radiation, depending on the gas emissivity, confirming the results obtained in [19]. For metallized propellant, the erosion rate has been found to decrease marginally when coupled wall reradiation and particle radiation effects are considered. Two simplified models have been adopted to evaluate the integral particle emissivity in metallized propellants, giving substantially different emissivity values at the throat. Nevertheless, the throat erosion rate differences obtained for the two models are less than 3% of the baseline value without radiation. The primary effect of the particle radiation is the modification of the wall temperature profile. The weak dependence of the erosion rate on the change in wall temperature in the case of the diffusion-limited regime explains the insensitivity of the throat erosion to the particle radiation.

Thus, surface roughness enhances the erosion rate for both propellants by directly increasing the convective heat flux and species diffusivity at the wall due to enhanced near-wall turbulence. Radiation, however, directly influences only the wall temperature, which in turn influences the species diffusivity indirectly. Thus, it is clear that, with respect to radiation, the kinetically controlled nonmetallized propellant experiences more erosion-rate changes than the diffusion-limited metallized propellant. Analyses on smooth and rough surfaces, together with gas/particle radiation for both metallized and nonmetallized propellants, show that the trend in throat erosion variation caused by the gas/particle radiation is not affected much when surface roughness is considered, indicating a loose coupling between the influence of roughness and radiation. This suggests that the analysis of the two phenomena could be carried out separately without producing significant errors in the evaluation of the erosion rate variation.

References

- [1] Kowal, T. J., "Thermal Protection System (Heat Shield) Development: Advanced Development Project," Commercial Human Spaceflight Symposium, NASA Rept. JSC-CN-21831, Houston, TX, Oct. 2010.
- [2] Bianchi, S., Serraglia, F., Giliberti, F., and Betti, F., "Vega Solid Rocket Motors Development and Qualification," AIAA Paper 2010-7084, 2010.
- [3] Delaney, L. J., Eagleton, L. C., and Jones, W. H., "A Semiquantitative Prediction of the Erosion of Graphite Nozzle Inserts," *AIAA Journal*, Vol. 2, No. 8, 1964, pp. 1428–1433. doi:10.2514/3.2570
- [4] McDonald, A. J., and Hedman, P. O., "Erosion of Graphite in Solid-Propellant Combustion Gases and Effects on Heat Transfer," *AIAA Journal*, Vol. 3, No. 7, 1965, pp. 1250–1257. doi:10.2514/3.3117

- [5] Kuo, K. K., and Keswani, S. T., "A Comprehensive Theoretical Model for Carbon–Carbon Composite Nozzle Recession," *Combustion Science and Technology*, Vol. 42, Nos. 3–4, 1985, pp. 145–164. doi:10.1080/00102208508960374
- [6] Kuo, K. K., and Keswani, S. T., "Validation of an Aerothermochemical Model for Graphite Nozzle Recession and Heat-Transfer Processes," *Combustion Science and Technology*, Vol. 47, Nos. 3–4, 1986, pp. 177–192. doi:10.1080/00102208608923872
- [7] Acharya, R., and Kuo, K. K., "Effect of Pressure and Propellant Composition on Graphite Rocket Nozzle Erosion Rate," *Journal of Propulsion and Power*, Vol. 23, No. 6, 2007, pp. 1242–1254. doi:10.2514/1.24011
- [8] Acharya, R., and Kuo, K. K., "Effect of Reaction Kinetic Schemes on Graphite Rocket Nozzle Erosion Rates," *International Journal of Energetic Materials and Chemical Propulsion*, Vol. 9, No. 1, 2010, pp. 71–90. doi:10.1615/IntJEnergeticMaterialsChemProp.v9.i1.50
- [9] Thakre, P., and Yang, V., "Chemical Erosion of Carbon–Carbon/Graphite Nozzles in Solid-Propellant Rocket Motors," *Journal of Propulsion and Power*, Vol. 24, No. 4, 2008, pp. 822–833. doi:10.2514/1.34946
- [10] Thakre, P., and Yang, V., "Mechanical Erosion of Nozzle Material in Solid-Propellant Rocket Motors," AIAA Paper 2010-615, 2010.
- [11] Bianchi, D., Nasuti, F., and Martelli, E., "Coupled Analysis of Flow and Surface Ablation in Carbon–Carbon Rocket Nozzles," *Journal of Spacecraft and Rockets*, Vol. 46, No. 3, 2009, pp. 492–500. doi:10.2514/1.40197
- [12] Bianchi, D., Nasuti, F., Onofri, M., and Martelli, E., "Thermochemical Erosion Analysis for Graphite/Carbon–Carbon Rocket Nozzles," *Journal of Propulsion and Power*, Vol. 27, No. 1, 2011, pp. 197–205. doi:10.2514/1.47754
- [13] Bianchi, D., and Nasuti, F., "Carbon–Carbon Nozzle Erosion and Shape Change in Full-Scale Solid-Rocket Motors," *Journal of Propulsion and Power*, Vol. 28, No. 4, 2012, pp. 820–830. doi:10.2514/1.58842
- [14] Turchi, A., Bianchi, D., Nasuti, F., and Onofri, M., "A Numerical Approach for the Study of the Gas-Surface Interaction in Carbon–Phenolic Solid Rocket Nozzles," *Aerospace Science and Technology*, Vol. 27, No. 1, 2013, pp. 25–31. doi:10.1016/j.ast.2012.06.003
- [15] Bianchi, D., Turchi, A., Nasuti, F., and Onofri, M., "Chemical Erosion of Carbon–Phenolic Rocket Nozzles with Finite-Rate Surface Chemistry," *Journal of Propulsion and Power*, Vol. 29, No. 5, 2013, pp. 1220–1230. doi:10.2514/1.B34791
- [16] Thakre, P., and Yang, V., "Chemical Erosion of Refractory-Metal Nozzle Inserts in Solid-Propellant Rocket Motors," *Journal of Propulsion and Power*, Vol. 25, No. 1, 2009, pp. 40–50. doi:10.2514/1.37922
- [17] Duffa, G., Vignoles, G. L., Goyh  n  che, J., and Aspa, Y., "Ablation of Carbon-Based Materials: Investigation of Roughness Set-Up from Heterogeneous Reactions," *International Journal of Heat and Mass Transfer*, Vol. 48, No. 16, 2005, pp. 3387–3401. doi:10.1016/j.ijheatmasstransfer.2005.02.036
- [18] Vignoles, G. L., Lachaud, J., Aspa, Y., and Goyh  n  che, J., "Ablation of Carbon-Based Materials: Multiscale Roughness Modelling," *Composites Science and Technology*, Vol. 69, No. 9, 2009, pp. 1470–1477. doi:10.1016/j.compscitech.2008.09.019
- [19] Thakre, P., and Yang, V., "Effect of Surface Roughness and Radiation on Graphite Nozzle Erosion in Solid Rocket Motors," *Journal of Propulsion and Power*, Vol. 28, No. 2, 2012, pp. 448–451. doi:10.2514/1.57841
- [20] Auipoix, B., and Spalart, P. R., "Extensions of the Spalart–Allmaras Turbulence Model to Account for Wall Roughness," *International Journal of Heat and Fluid Flow*, Vol. 24, No. 4, 2003, pp. 454–462. doi:10.1016/S0142-727X(03)00043-2
- [21] Anderson, J. D., Jr., *Hypersonic and High-Temperature Gas Dynamics*, 2nd ed., AIAA Education Series, AIAA, Reston, VA, 2006, pp. 712–719.
- [22] McBride, B. J., and Gordon, S., "Computer Program for Calculation of Complex Chemical Equilibrium Compositions and Applications: 1. Analysis," NASA John H. Glenn Research Center, NASA Reference Publ. RP-1311, Cleveland, OH, Oct. 1994.
- [23] Bird, R. B., Stewart, W. E., and Lightfoot, E. D., *Transport Phenomena*, Wiley, New York, 1960, pp. 563–572.
- [24] Sutton, K., and Gnoffo, P. A., "Multi-Component Diffusion with Application to Computational Aerothermodynamics," AIAA Paper 1998-2575, 1998.
- [25] Chelliah, H., Makino, A., Kato, I., Araki, N., and Law, C., "Modeling of Graphite Oxidation in a Stagnation-Point Flow Field Using Detailed Homogeneous and Semiglobal Heterogeneous Mechanisms with Comparisons to Experiments," *Combustion and Flame*, Vol. 104, No. 4, 1996, pp. 469–480. doi:10.1016/0010-2180(95)00151-4
- [26] Bradley, D., Dixon-Lewis, G., din Habik, S. E., and Mushi, E., "The Oxidation of Graphite Powder in Flame Reaction Zones," *Symposium (International) on Combustion*, Vol. 20, No. 1, 1985, pp. 931–940. doi:10.1016/S0082-0784(85)80582-8
- [27] Spalart, P. R., "Trends in Turbulence Treatments," AIAA Paper 2000-2306, 2000.
- [28] Dirling, R. B. J., "A Method for Computing Roughwall Heat Transfer Rates on Reentry Nosetips," AIAA Paper 1973-763, 1973.
- [29] Nikuradse, J., "Laws of Flow in Rough Pipes," NACA TM-1292, 1950.
- [30] Spalart, P. R., and Allmaras, S. R., "A One-Equation Turbulence Model for Aerodynamic Flow," *La Recherche Aeronautique*, Vol. 1, 1994, pp. 5–21.
- [31] Hosni, M., Coleman, H. W., and Taylor, R. P., "Measurements and Calculations of Rough-Wall Heat Transfer in the Turbulent Boundary Layer," *International Journal of Heat and Mass Transfer*, Vol. 34, Nos. 4–5, 1991, pp. 1067–1082. doi:10.1016/0017-9310(91)90017-9
- [32] Hosni, M., Coleman, H. W., Garner, J. W., and Taylor, R. P., "Roughness Element Shape Effects on the Heat Transfer Skin Friction in Rough-Wall Turbulent Boundary Layer," *International Journal of Heat and Mass Transfer*, Vol. 36, No. 1, 1993, pp. 147–153.
- [33] Pearce, B. E., "Radiative Heat Transfer Within a Solid-Propellant Rocket Motor," *Journal of Spacecraft and Rockets*, Vol. 15, No. 2, 1978, pp. 125–128. doi:10.2514/3.28003
- [34] Murphy, A., and Kwong, K., "Nozzle Control Bulletin," NASA TM-75-86, 1975.
- [35] Dombrovsky, L. A., *Radiation Heat Transfer in Disperse Systems*, Begell House, New York, 1996.
- [36] Evans, B., Kuo, K. K., Ferrera, P. J., Moore, J. D., Kutzler, P., and Boyd, E., "Nozzle Throat Erosion Characterization Study Using a Solid-Propellant Rocket Motor Simulator," AIAA Paper 2007-5776, 2007.
- [37] Geisler, R. L., and Beckam, C. W., "The History of the Bates Motors at the Air Force Rocket Propulsion Laboratory," AIAA Paper 1998-3981, 1998.
- [38] Williams, S. D., and Curry, D. M., "Thermal Protection Materials: Thermophysical Property Data," NASA Reference Publ. RP-1289, 1992.
- [39] Sutton, G. P., and Biblarz, O., *Rocket Propulsion Elements*, 7th ed., Wiley-Interscience, New York, 2001, p. 499.
- [40] Laganelli, A. L., and Nestler, D., "Surface Ablation Patterns: A Phenomenology Study," *AIAA Journal*, Vol. 7, No. 7, 1969, pp. 1319–1325. doi:10.2514/3.5340
- [41] Williams, E. P., "Experimental Studies of Ablation Surface Patterns and Resulting Roll Torques," *AIAA Journal*, Vol. 9, No. 7, 1971, pp. 1315–1321. doi:10.2514/3.49941
- [42] Frankle, R., and Lebedzik, J., "A New Technique for Characterizing Surface Roughness," *CPIA Publications*, No. 328, 1980, pp. 415–431.
- [43] Modest, M. F., *Radiative Heat Transfer*, 2nd ed., Academic, New York, 2003, pp. 339–346.